Label-free imaging of biomolecules in food products using stimulated Raman microscopy

Maarten B. J. Roeffaers,[a] Xu Zhang,[a,b] Christian W. Freudiger,[a,c] Brian G. Saar,[a] Marjolein van Ruijven,[d] Gerard van Dalen,[d] Chunhong Xiao,[e] and X. Sunney Xie[a]
[a]Harvard University, Department of Chemistry and Chemical Biology, Cambridge, Massachusetts 02138
[b]Harvard University, School of Engineering and Applied Sciences, Cambridge, Massachusetts 02138
[c]Harvard University, Department of Physics, Cambridge, Massachusetts 02138
[d]Unilever Research and Development, Advanced Measurement and Data Modelling, 3133AT Vlaardingen, Netherlands
[e]Unilever Research and Development, Advanced Measurement and Data Modelling, Trumbull, Connecticut 06611

Abstract. The development of methods that allow microscale studies of complex biomaterials based on their molecular composition is of great interest to a wide range of research fields. We show that stimulated Raman scattering (SRS) microscopy is an excellent analytical tool to study distributions of different biomolecules in multiphasic systems. SRS combines the label-free molecular specificity of vibrational spectroscopy with an enhanced sensitivity due to coherent excitation of molecular vibrations. Compared to previous imaging studies using coherent anti-Stokes Raman scattering microscopy, the main advantage of SRS microscopy is the absence of the unwanted nonresonant background, which translates into a superior sensitivity and undistorted vibrational spectra. We compare spectra of complex materials obtained with stimulated Raman scattering and spontaneous Raman scattering in the crowded fingerprint region. We find that, as expected, there is excellent correspondence and that the SRS spectra are free from interference from background fluorescence. In addition, we show high-resolution imaging of the distributions of selected biomolecules, such as lipids and proteins, in food products with SRS microscopy. [DOI: 10.1117/1.3516591]

Keywords: nonlinear optical microscopy; stimulated Raman spectroscopy; label-free microscopy.

Paper 10468R received Aug. 23, 2010; revised manuscript received Sep. 29, 2010; accepted for publication Sep. 30, 2010; published online Feb. 2, 2011.

1 Introduction

Optical microscopy is valuable for unraveling the complex organization of biomaterials because it allows nondestructive imaging with a high spatiotemporal resolution. Fluorescence microscopy is currently the most widely used type of optical microscopy in biomedical[1] and food research[2,3] because of its sensitivity and molecular specificity. However, fluorescence studies require staining or the use of fluorogenic reactants, which is not always possible and may even perturb the system under investigation. Recently, significant research effort has been focused on the development of label-free microscopy with chemical contrast. Vibrational spectroscopy, based on infrared absorption or Raman scattering, gives access to a variety of intrinsic molecular signatures, avoiding the need for labeling. Unfortunately, the spatial resolution of infrared microscopy is poor because of the long wavelengths, and the penetration into aqueous samples is limited by strong water absorption in the infrared. Raman spectroscopy with visible or near-infrared (NIR) wavelengths offers high resolution in aqueous samples, but the Raman scattering efficiency is extremely low, necessitating high laser power and long integration times to achieve good sensitivity. This limits the detailed observation of microscopic features.

The weak Raman signals can be strongly enhanced by using nonlinear coherent excitation. This makes it possible to image molecular distributions with submicron resolution and imaging speeds up to video rate by targeting isolated vibrational resonances.[4,5] This has been the main driving force behind the development of coherent anti-Stokes Raman scattering (CARS) microscopy during the last decade. The major challenge in CARS microscopy is that the recorded signal suffers from a strong nonresonant background due to the electronic response of molecules in the sample. This background limits the sensitivity of CARS by overwhelming weak resonant signals and distorting the vibrational spectrum through interference. The well-isolated CH_2-stretching mode of lipids at 2845 cm^{-1} has been extensively utilized in CARS, but the spectral interference limits the applicability of CARS microscopy to target vibrational signatures in the densely populated fingerprint region. Some advanced CARS-based imaging techniques, such as polarization sensitive CARS,[6] time-resolved CARS[7], interferometric CARS,[8] and multiplex CARS,[9–11] have been developed to minimize the nonresonant background. However, these techniques either sacrifice signal or require postprocessing and do not allow the direct imaging of molecular distributions in complex materials. This only became possible recently with the development of stimulated Raman scattering (SRS) microscopy, which offers high sensitivity and does not suffer from the nonresonant background.[12] With the currently available lasers, it is possible to get direct access to a whole range of vibrational frequencies with SRS, including those in the fingerprint region. A major advantage of SRS compared to CARS is that it has the same spectral response as the spontaneous Raman signal even in

Address all correspondence to: X. Sunney Xie, Harvard University, Department of Chemistry and Chemical Biology, 12 Oxford Street, Cambridge, Massachusetts 02138; Tel: 617-496-9925; Fax: 617-496-8709; E-mail: xie@chemistry.harvard.edu

1083-3668/2011/16(2)/021118/6/$25.00 © 2011 SPIE

congested spectral regions and hence enables selective imaging of the different biomolecules, such as lipids and proteins, without the need for data processing. For this study, we used different food products that commonly appear as complex multiphasic systems because many organics are not miscible with water.[13] These emulsions are major structure and structure-forming units within many foods products. The microstructure of emulsions determines, to a large extent, their appearance, texture, taste, and handling properties. Techniques to image these structures provide important feedback to control and optimize process technologies. SRS microscopy is an effective label-free analytical tool to study the distribution and organization of the constituents in such emulsion systems by specifically targeting the different vibrational modes of molecules at submicron resolution.

2 Materials and Methods

2.1 *Sample Preparation*

Three commercial food samples were used in this study: mayonnaise (Hellmann's® Real Mayonnaise, Unilever, Englewood Cliffs), cheese (Swiss Cheese, Trader Joe's, Monrovia, California), and soy-based drink (AdeZ, Unilever Englewood Cliffs). We prepared 120-μm-thick samples between two No. 1 coverslides (VWR, Radnor, Pennsylvania) by using a spacer made from double-sided adhesive sheets (SecureSeal SA-S-1L, Grace Bio-labs, Bend, Oregon). All experiments were performed at room temperature.

2.2 *Stimulated Raman Scattering Microscope (Fig. 1)*

Stimulated excitation of the Raman scattering occurs when the difference in energy between two laser beam matches a particular molecular vibration. This process increases the intensity of the Stokes beam and reduces the intensity of the pump beam. Because this intensity gain and loss are very small compared to the intensity of the applied lasers ($<10^{-4}$), it is buried within the laser noise. High-frequency intensity modulation (megahertz frequencies) of the Stokes beam is applied to separate the stimulated Raman effect from the laser noise occurring at much lower frequencies (Hertz to kilohertz). The laser source of this microscopy setup is a 1064-nm Nd:YVO_4 laser (picoTRAIN, High-Q, Watertown, Massachusetts) that delivers 7 ps pulses at a 76-MHz repetition rate. One part of the output is frequency doubled to 532 nm, which pumps an optical parametric oscillator (OPO) (Levante Emerald, APE-Berlin, Berlin, Germany). A second output directly provides the remaining part of the 1064-nm beam. The signal beam of the OPO is tunable between 680 and 1010 nm. In this SRS setup, the OPO output is used as the pump beam for the SRS experiment, which in combination with the 1064-nm output of the Nd:YVO_4 laser (Stokes beam) probes the Raman shifts from >3500 to 500 cm^{-1}. The idler beam of the OPO is blocked with filter (CARS 890/220m, Chroma Technology, Bellow Falls, Vermont). A home-built Pockel cell based on a pair of 2×2×10 mm rubidium titanyl phosphate crystals (Raicol Crystals, Ltd., Yehud, Israel) combined with a polarizer is used to modulate the Stokes beam intensity. The modulation frequency of 10.4 MHz is directly provided by

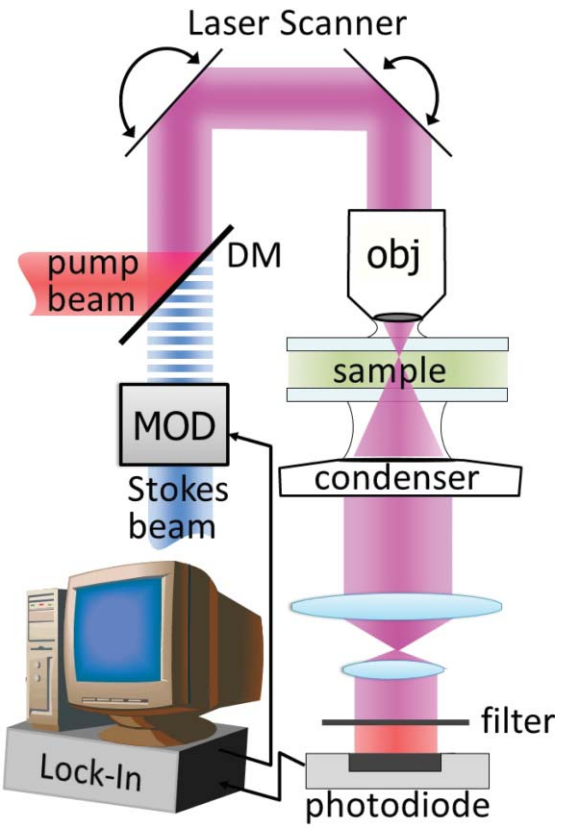

Fig. 1 Schematic of the SRS microscope. After combining the pump and Stokes beam with a dichroic mirror (DM), the laser beam is scanned over the sample in two dimensions. The transmitted light is collected with a condenser and after removal of the Stokes beam detected by a silicon photodiode. A lock-in amplifier supplies the modulation frequency to the Pockel cell in the Stokes beam, and this same frequency is used to demodulate the detected signal.

the lock-in amplifier (SR844RF, Stanford Research Systems, Sunnyvale, California). The pump and Stokes beam are spatially overlapped using a dichroic mirror (1064 DCRB, Chroma Technology, Bellow Falls, Vermont), and a manual delay stage is used to overlap both pulse trains in time.

These two spatially and temporally overlapped laser beams are directed into an upright Olympus laser-scanning microscope (BX61WI/FV300, Olympus, Pittsburgh, Pennsylvania) optimized for NIR transmission. The sample is illuminated through a 60×1.2-NA (Numerical Aperture) water objective (UPlanApo/IR, Olympus, Pittsburgh, Pennsylvania), and care is taken that the beam diameter matches the size of the back aperture of the objective. The transmitted light is collected with a 1.4-NA oil condenser (Nikon, Melville, New York), which is aligned for Koehler illumination. After passing a telescope, the transmitted light is spectrally filtered by a bandpass filter (CARS890/220M, Chroma Technology, Bellow Falls, Vermont) and detected by a large-area photodiode (FDS1010, Thorlabs, Newton, New Jersey) with a reversed bias of 64 V. Before measuring the modulation transfer with a high-frequency lock-in amplifier (SR844RF, Stanford Research Systems, Sunnyvale, California), an electronic bandpass filter (BBP-10.7, Mini-Circuits, Brooklyn, New York) is used. The analog output of the lock-in amplifier is fed into the input of the

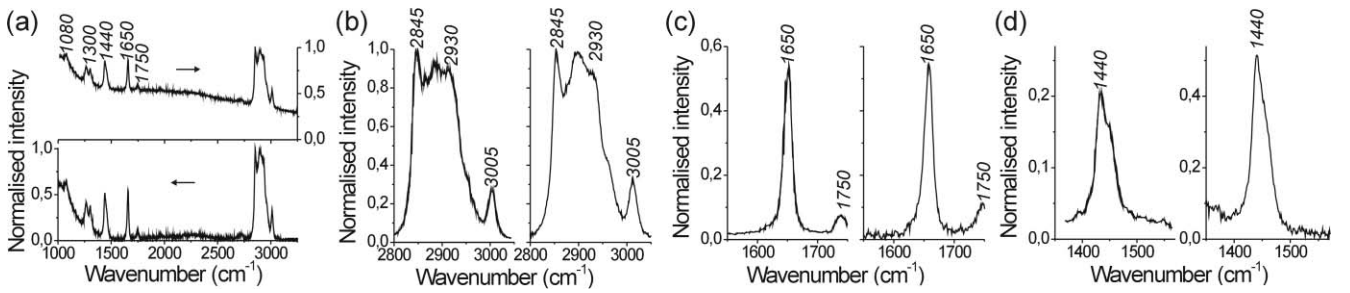

Fig. 2 Comparison between spontaneous and stimulated Raman spectrum of a mayonnaise sample: (a) Spontaneous Raman spectrum before (top) and after (bottom) subtraction of the fluorescence background and (b)–(d) SRS spectrum (left) and spontaneous Raman spectrum (right) measured at different regions of the vibrational spectrum.

microscope's A/D-converter. Images were taken at 42 μs/pixel or 11 s for a 512×512–pixel image.

Recording of SRS spectra was performed using a home-built LabVIEW routine. This software automatically scans the output of the OPO over a 10–20 nm range by changing the orientation of the in-cavity Lyot filter and simultaneously records the SRS signal intensity directly from the analog output of the lock-in amplifier. Phase-matching temperature and cavity length of the OPO were set manually and remain unchanged during the tuning.

2.3 *Spontaneous Raman Spectroscopy*

The spontaneous Raman spectra were acquired at room temperature using a confocal laser Raman spectrometer (Labram HR800, Horiba Jobin Yvon Inc., Edison, New Jersey). A 10-mW 633-nm HeNe laser was used to excite the sample through a 50×, 0.75 NA objective (MPlan N, Olympus, Pittsburgh, Pennsylvania). A polychromator with 600 lines/mm was used to disperse the light onto the CCD camera. The total data acquisition was performed during 40 s, and the background was subtracted using the LabSpec software.

3 Results and Discussion

3.1 *SRS Microspectroscopy in Mayonnaise*

One well-known multiphasic food product is mayonnaise, which is an oil-in-water emulsion. The overall properties of the end product are determined not only by the total fat/water ratio, but also by the distribution and the size of the lipid droplets.[13,14] The sample used in this study is a full-fat mayonnaise, which contains 77% lipids on a weight basis, of which the large majority (85%) is unsaturated.

First, a traditional spontaneous Raman spectrum was recorded with a total integration time of 40 s. Figure 2(a) shows this Raman spectrum of mayonnaise before and after correction for the inherent fluorescence background of the sample. Because mayonnaise largely consists of lipids, it is fairly easy to attribute the major peaks to specific chemical bonds and their vibrational modes.[15] Most clearly recognizable is the strong Raman signal stemming from the C–H stretching in the region between 2800–3050 cm^{-1}. A detailed analysis of this region shows that it consists of several (partially) overlapping bands [Fig. 2(b)]. In particular, the band around 2845 cm^{-1} originates from paraffinic C–H vibrations [$\nu(CH_2)$], the band centered at 2930 cm^{-1} originates from C–H vibrations in terminal methyl groups [$\nu(CH_3)$], and the peak at 3005 cm^{-1} is the result of C–H vibrations at unsaturated C=C bonds of the lipids [ν(=C–H)].[14,15] Other very strong vibrational modes of C–H bonds appear in the fingerprint region (<2000 cm^{-1}) [Figs. 2(a)–2(d)]. The peaks at 1445 and 1300 cm^{-1} originate respectively from $\rangle CH_2$ scissoring [$\delta(CH_2)$] and the in-phase methylene twisting mode. In addition to C–H bond vibrations, the 1750-cm^{-1} resonance results from the C=O stretching [(ν(C=O)] of the ester groups present in glycerides, the 1655-cm^{-1} peak can be attributed to C=C vibrations [ν(C=C)] of unsaturated lipids, and the peak at 1080 cm^{-1} can be linked to skeletal C–C vibration [ν(C–C)] of the lipids.[14,15] All these vibrational resonances show up as distinctive peaks that are directly related to the lipids in mayonnaise. The Raman spectrum of water [ν(O-H)] is generally known to consist of a very broad peak centered around 3500 cm^{-1} that extends almost into the C–H region.

In the next step, we acquired SRS spectra of the same mayonnaise sample. A LabVIEW program was used to acquire the datapoints with, 1 cm^{-1} per step by automated tuning of the OPO's Lyot filter, and the acquisition time for every datapoint was 100 ms. Figures 2(b)–2(d) compare the stimulated and spontaneous Raman scattering spectra for three different vibrational regions. These spectra clearly show that SRS does not suffer from the interference with the nonresonant background such as coherent anti-Stokes Raman scattering. Instead of the dispersive line shapes of CARS spectra, SRS spectra are identical to the spontaneous Raman spectra. Another major benefit of SRS is that it is not hindered by background fluorescence; no fluorescence background corrections had to be performed as was done for the spontaneous Raman spectrum in Fig. 2. Because of the similarity in spectral response between SRS and spontaneous Raman scattering it is safe to use the well-known, molecularly specific vibrational frequency of a species of interest for coherent excitation. Because the SRS signal is linear with concentration, local variations in signal intensity can be directly related to differences in local concentration. This approach was used to visualize the water and lipid distribution in mayonnaise [Figs. 3(a)–3(d)]. Figures 3(a) and 3(b) show the lipid distribution based on the paraffinic CH_2 stretching (2845 cm^{-1}) and the $\rangle CH_2$ scissoring (1440 cm^{-1}). Both images are representative for unsaturated and saturated lipids and show, as expected, a similar distribution. In Fig. 3(c), the distribution of unsaturated lipids is visualized by targeting the peak at 3005 cm^{-1}. Note that identical information regarding the lipid distribution can also be obtained using different vibrational modes, such as the

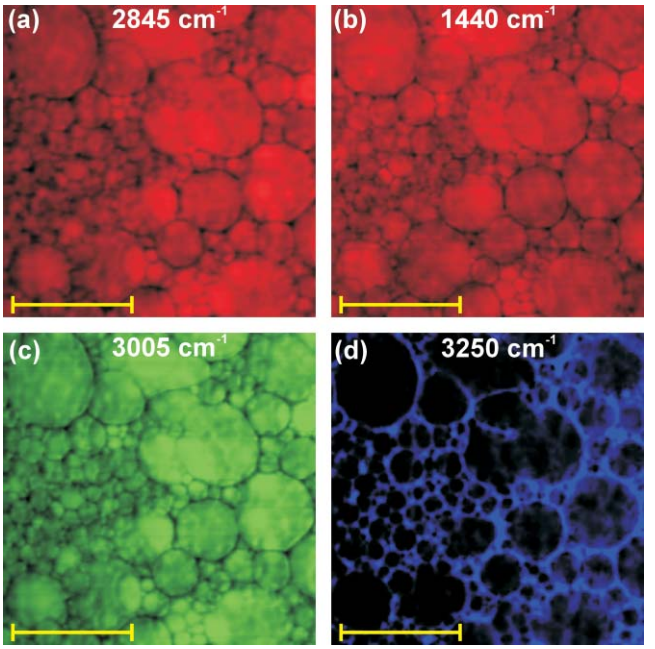

Fig. 3 SRS micrographs (52×52 μm^2) of mayonnaise. (a)–(c) SRS images at different CH_2 vibrational resonances using: (a) 2845 cm^{-1} and (b) 1440 cm^{-1}, (c) SRS images of the unsaturated lipid distribution recorded at 3005 cm^{-1}, and (d) water distribution measured at 3250 cm^{-1}. Scale bar in the images is 20 μm.

in-phase methylene twisting mode (1303 cm^{-1}) and the C=C stretching at 1655 cm^{-1} (data not shown). As expected for mayonnaise, the unsaturated and saturated lipids are colocalized within large lipid droplets, which range in size from 1 to 15 μm diam. The inverse image [Fig. 3(d)] is obtained when recording the water distribution at 3250 cm^{-1}. The two complementary images nicely visualize the molecular distribution in this oil in water emulsion. These measurements show that with SRS microscopy we can selectively visualize the different components of a multiphase material such as mayonnaise, without adding labels and with a time resolution that is more than three orders of magnitude faster than typical spontaneous Raman imaging.

3.2 *SRS Imaging of Proteins, Lipids, and Water in Cheese and Soy Drinks*

In general, food products have a more complex chemical composition. In addition to oil and water, significant amounts of proteins and carbohydrates are also often present. We, for example, examined cheese and a soy-based drink, which contain significant amounts of proteins, lipids, and water. In this particular semi-hard Swiss cheese sample, the listed content is 28 wt % lipids and 32 wt % proteins. Figure 4(a) shows the spontaneous Raman spectrum after correction for the background. Noteworthy is the absence of the 3005 cm^{-1} resonance peak in the CH stretching region, which indicates that virtually the whole fat content of this cheese consists of saturated lipids. Because of the presence of large quantities of proteins in cheese compared to the mayonnaise sample, there is also a relative increase of the terminal methyl group [$\nu(CH_3)$] vibration at 2930 cm^{-1} with respect to that at 2845 cm^{-1} stemming from aliphatic $\nu(CH_2)$ resonance. Furthermore, the aromatic amino acids in

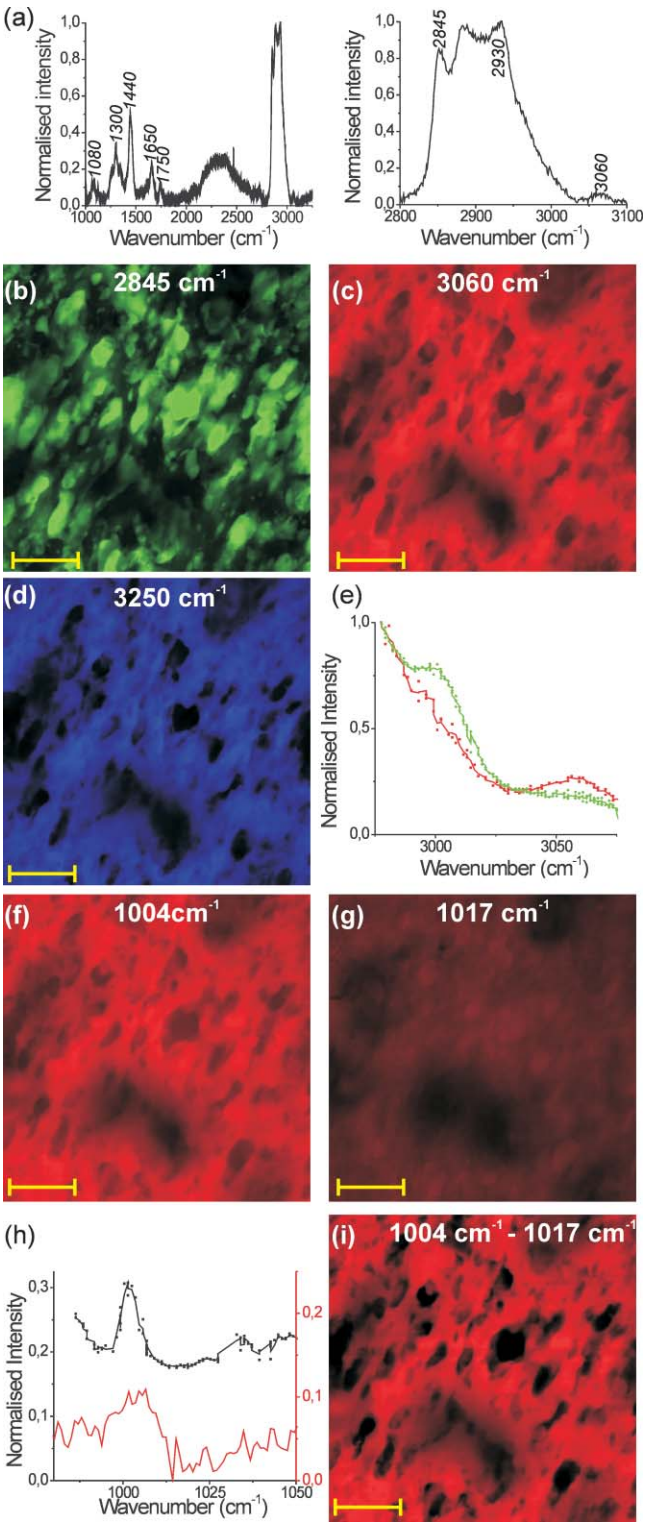

Fig. 4 Vibrational characterization of biomolecules in cheese sample. (a) Spontaneous Raman spectrum. (b)–(d) SRS images of the distribution of (b) lipids (2845 cm^{-1}), (c) protein (3060 cm^{-1}) and (d) water (3250 cm^{-1}), (e) SRS spectrum of the whole area (red) and of the lipid phase (green), (f) SRS image of protein distribution by targeting the 1004-cm^{-1} ring breathing resonance of phenylalanine, (g) SRS micrograph measured at 1017 cm^{-1}, (h) comparison between the spontaneous Raman spectrum after fluorescence subtraction (red) and the SRS spectrum around 1004 cm^{-1}, and (i) image obtained by subtracting the signal detected at 1004 and 1017 cm^{-1}. The scale bar in the SRS micrographs is 20 μm.

proteins such as phenylalanine and tryptophan give rise to a new peak at 3060 cm^{-1}, which is a signature for aromatic C–H vibrations. Because of these aromatic amino acids, there should be another very distinctive peak in the fingerprint region at 1004 cm^{-1} originating from the ring-breathing mode of phenylalanine. Even though there are almost no unsaturated lipids present in this sample, there is still a very strong resonance at 1650 cm^{-1}. This signal is generated by the ν(C=O) in the amide bonds of proteins is overlapping with the signal stemming from C=C bonds in unsaturated lipids. When using the 1650 cm^{-1} peak for coherent Raman imaging, care must be taken to analyze the relative contributions of lipids and proteins in this frequency range.

By using these different distinctive vibrational resonances, SRS allows selective visualization of the protein, lipid and water distribution. Figures 4(b)–4(d) compares the SRS images of a 95×95–μm^2 region taken for different C–H vibrations. The images taken at 2845 cm^{-1}, specific for the lipid distribution [Fig. 4(b)], and at 3060 cm^{-1}, specific for the protein distribution [Fig. 4(c)], show an inverse contrast, indicating that this cheese consists of two well-separated phases.[16,17] The image taken at the water tail [Fig. 4(d)] at 3250 cm^{-1}, shows the same distribution as the protein channel, suggesting that water and proteins make up one phase of the cheese material and lipids can be found in a separate phase. To demonstrate that the broad water resonance cannot explain the contrast at 3060 cm^{-1}, a SRS spectrum was recorded to prove that in this case the signal measured at 3060 cm^{-1} is representative for the protein distribution. An overall spectrum was collected by scanning rapidly over the whole image area (95×95 μm^2) while recording the spectrum, 1 cm^{-1}/100 ms. This spectrum [Fig. 3(e)] clearly shows the presence of a resonant peak at 3060 cm^{-1}, specific for aromatic amino acids in proteins. When focusing specifically on a fat globule, a small bump due to the presence of a small amount of unsaturated lipids can be resolved. Another useful vibrational resonance to specifically target the protein distribution is the phenylalanine peak at 1004 cm^{-1}; Fig. 4(f) shows the protein distribution as determined at this phenylalanine peak. This image compares well to Fig. 4(c) recorded at 3060 cm^{-1}; however, the zones where lipids are present show some residual intensity. This residual SRS intensity can be attributed to the multitude of vibrational resonances that are close by and partly overlapping. This becomes even more apparent when tuning the pump wavelength less than 2 nm away when recording at 1017 cm^{-1} [Fig. 4(g)]. This image clearly shows a vibrationally resonant signal that clearly has a different distribution than the one recorded at the phenylalanine peak. The presence of multiple vibrational resonances can also be seen as a broad offset of this phenylalanine peak in the SRS spectrum [Fig. 4(h)]. In contrast to the spontaneous Raman spectrum, where this peak is only weakly present, the SRS spectrum shows a significant resonance intensity. To minimize the contribution from nearby vibrational resonances, the signal obtained at 1017 cm^{-1} was subtracted from that at 1004 cm^{-1} [Fig. 4(i)]. This image shows a lipid phase that is virtually free of any protein content similar to that obtained at 3060 cm^{-1} [Fig. 4(c)].

Because SRS microscopy allows fast image acquisition at one vibrational frequency and tuning between the different bands can be performed reasonably fast, this approach can also be used to image biomolecular distributions in liquid samples, such as a commercial soy-based drink; these drinks are oil-in-water emulsions in which the continuous phase is formed by complex protein dispersion. The lipid distribution was determined by measuring the SRS signal at 2845 cm^{-1} [Fig. 5(a)], the protein content was determined by targeting the phenylalanine peak [1004 cm^{-1}, Fig. 5(b)], and for the water distribution the SRS signal was measured at 3400 cm^{-1} [Fig. 5(c)]. These images and the combined multicolor image [Fig. 5(d)] clearly show that this sample has a more complex multiphasic structure.

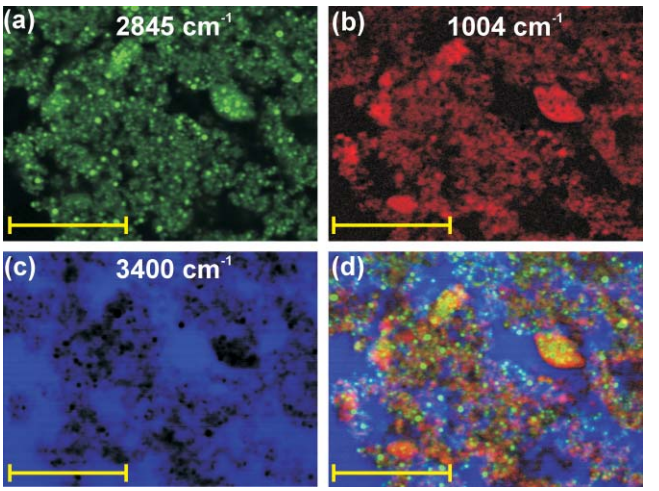

Fig. 5 SRS image of the distribution of (a) lipids, (b) protein, and (c) water in a soy-based drink (54 x 40 μm^2 area). (d) Multicolor image showing the combined distribution of all three components. Scale bar is 20 μm.

4 Conclusion

We have used SRS as a noninvasive tool to map distributions of specific biomolecules in food products at the submicronscale. SRS microscopy combines high sensitivity resulting from the coherent excitation of molecular vibrations with easily interpretable contrast because its spectral response is identical to spontaneous Raman spectroscopy. This makes fast and quantitative imaging available using the well-known vibrational frequencies throughout the whole vibrational spectrum. This contribution is focused on imaging lipids, proteins, and water, using both the high wavenumber CH and OH stretching region as well as a number of fingerprint bands. It was recently shown that SRS microscopy also allows direct targeting of sugars such as cellulose and more complex biopolymers like lignin in plant materials.[18] Thus, SRS microscopy is an ideal tool to study biomolecular distributions in a wide range of research areas based on the full information of Raman spectroscopy.

Acknowledgments

M.B.J.R. thanks the Fonds voor Wetenschappelijk Onderzoek for a postdoctoral fellowship and acknowledges the support from the Belgian American Educational Foundation and the Fulbright Commission–Belgium. C.W.F. acknowledges a Ph.D. Fellowship from Boehringer Ingelheim Fonds. The work conducted at Harvard is funded by Unilever.

References

1. J. Pawley, *Handbook of Biological Confocal Microscopy*, Springer, New York (2006).
2. J. C. G. Blonk and H. Van Aalst, "Confocal scanning light-microscopy in food research," *Food Res. Int.* **26**(4), 297–311 (1993).
3. G. Van Dalen, "Determination of the water droplet size distribution of fat spreads using confocal scanning laser microscopy," *J. Microsc.* **208**(2), 116–133 (2002).
4. J. X. Cheng and X. S. Xie, "Coherent anti-Stokes Raman scattering microscopy: instrumentation, theory, and applications," *J. Phys. Chem. B* **108**(3), 827–840 (2004).
5. C. L. Evans and X. S. Xie, "Coherent anti-stokes Raman scattering microscopy: chemical imaging for biology and medicine," *Annu. Rev. Anal. Chem.* **1**, 883–909 (2008).
6. J. X. Cheng, L. D. Book, and X. S. Xie, "Polarization coherent anti-Stokes Raman scattering microscopy," *Opt. Lett.* **26**(17), 1341–1343 (2001).
7. A. Volkmer, L. D. Book, and X. S. Xie, "Time-resolved coherent anti-Stokes Raman scattering microscopy: Imaging based on Raman free induction decay," *Appl. Phy. Lett.* **80**(9), 1505–1507 (2002).
8. E. O. Potma, C. L. Evans, and X. S. Xie, "Heterodyne coherent anti-Stokes Raman scattering (CARS) imaging," *Opt. Lett.* **31**(2), 241–243 (2006).
9. J. X. Chen, A. Volkmer, L. D. Book, and X. S. Xie, "Multiplex coherent anti-stokes Raman scattering microspectroscopy and study of lipid vesicles," *J. Phys. Chem. B* **106**(34), 8493–8498 (2002).
10. E. M. Vartiainen, H. A. Rinia, M. Muller, and M. Bonn, "Direct extraction of Raman line-shapes from congested CARS spectra," *Opt. Express* **14**(8), 3622–3630 (2006).
11. J. P. R. Day, G. Rago, K. F. Domke, K. P. Velikov, and M. Bonn, "Label-free imaging of lipophilic bioactive molecules during lipid digestion by multiplex coherent anti-Stokes Raman scattering microspectroscopy," *J. Am. Chem. Soc.* **132**(24), 8433–8439 (2010).
12. C. W. Freudiger, W. Min, B. G. Saar, S. Lu, G. R. Holtom, C. W. He, J. C. Tsai, J. X. Kang, and X. S. Xie, "Label-free biomedical imaging with high sensitivity by stimulated Raman scattering microscopy," *Science* **322**(5909), 1857–1861 (2008).
13. M. Langton, E. Jordansson, A. Altskar, C. Sorensen, and A. M. Hermansson, "Microstructure and image analysis of mayonnaises," *Food Hydrocolloids* **13**(2), 113–125 (1999).
14. H. Sadeghi-Jorabchi, R. H. Wilson, P. S. Belton, J. D. Edwards-Webb, and D. T. Coxon, "Quantitative-analysis of oils and fats by fourier-transform Raman-spectroscopy," *Spectrochim. Acta Part A* **47**(9–10), 1449–1458 (1991).
15. S. Keller, T. Lochte, B. Dippel, and B. Schrader, "Quality-control of food with near-infrared excited raman-spectroscopy," *Fresenius. Anal. Chem.* **346**(6–9), 863–867 (1993).
16. G. G. Ribero, A. C. Rubiolo, and S. E. Zorrilla, "Microstructure of mozzarella cheese as affected by the immersion freezing in NaCl solutions and by the frozen storage," *J. Food Eng.* **91**(4), 516–520 (2009).
17. S. Gunasekaran and K. Ding, "Three-dimensional characteristics of fat globules in cheddar cheese," *J. Dairy Sci.* **82**(9), 1890–1896 (1999).
18. B. G. Saar, Y. Zeng, C. W. Freudiger, Y.-S. Liu, M. E. Himmel, X. S. Xie, and S.-Y. Ding, "Label-free, real-time monitoring of biomass processing with stimulated Raman scattering microscopy," *Angew. Chem. Int. Ed.* **49**(32), 5476–5479 (2010).